Saddle point solution of the Landau-Ginzburg-Wilson Hamiltonian for the McCoy-Wu Ising model

Xintian Wu*
Department of Physics, Beijing Normal University, Beijing, 100875, China

(Received 10 June 2018; published 20 June 2018)

The Landau-Ginzburg-Wilson Hamiltonian for the McCoy-Wu strip-random Ising model on a two-dimensional lattice is studied. In the Landau-Ginzburg-Wilson Hamiltonian, the random temperature only depends on one of the coordinates (x), the horizontal coordinate. The difference (rather than differential) saddle point equation is solved numerically. In the critical regime, there exist locally ordered regions, where the saddle point solutions are not zero. Due to the translational invariance in the vertical direction, the locally ordered regions are striplike in the vertical direction. In the excited state solutions, there exist horizontal domain walls across the locally ordered regions. It is found that these horizontal domain walls are stabilized by free-energy barriers due to the discreteness. The stability conditions for such domain walls are studied. Usually, the domain wall across multiple locally ordered regions can be stable. These multiple locally ordered regions form an elementary cluster. The criterion for multiple locally ordered regions forming an elementary cluster is obtained. At the saddle point level, we get an effective Hamiltonian in which the elementary clusters behave as Ising spins and are coupled with their neighbors. For the random temperatures with narrow uniform probability distributions, the distribution of elementary cluster size, the horizontal and vertical bonds between elementary clusters are calculated numerically. The vertical bonds are extremely strong and the horizontal bonds are extremely weak. The distribution of vertical bonds is exponential. There is an exponentially small probability of elementary clusters with extremely large size. These elementary clusters with extremely large size will cause the susceptibility divergent in a range of temperature. The random temperature with binary probability distributions is also studied. The qualitative properties are the same. The Griffiths-McCoy singularity in the saddle point solutions does not depend on the distribution of random temperature.

DOI: 10.1103/PhysRevB.97.224422

I. INTRODUCTION

The effects of quenched disorder on continuous phase transitions have been the subject of intense theoretical and experimental interest [1]. Due to the perfect correlation in the time direction, the disorder has strong effects on the quantum phase transition. The most interesting effect is the Griffiths-McCoy singularity, where several thermodynamic observables including the average susceptibility actually diverge in a finite region of the disordered phase rather than only at the critical point. The Griffiths-McCoy singularity was first discovered in the classical McCoy-Wu random Ising model [2–4], which can be mapped to a quantum model, the one-dimensional random field transverse-field Ising model. The McCoy-Wu model in zero magnetic field is partially exactly solvable with transfer-matrix-type methods [2–5]. A phenomenological optimal fluctuation theory of rare region effects was proposed to understand the Griffiths-McCoy singularity in the mid 1990's [6]. In the meantime, an asymptotically exact real-space renormalization group for the random transverse-field Ising model was achieved by Fisher [7,8]. Later, Griffiths-McCoy singularity in random transverse-field Ising model was studied intensively [9–12]. Griffiths-McCoy singularity was also found at percolation with linear defects [12] and the nonequilibrium phase transition in a disordered one-dimensional contact process [13–15]

The McCoy-Wu model consists of a nearest-neighbor Ising model on a rectangular lattice. For convenience, we rotate the original model 90°, all the vertical exchanges K are the same, while the horizontal bonds are identical to each other within each column but differ from column to column. In this paper, we shall study the saddle point equation of Landau-Ginzburg-Wilson Hamiltonian for the McCoy-Wu model. We find that the saddle point solution leads to the Griffiths-McCoy singularity.

The motivation of this work is twofold. On the one hand, the Landau-Ginzburg-Wilson Hamiltonian is a general framework in studying critical phenomena. However, the conventional field-theoretic or replica description fails to describe the Griffiths-McCoy singularity in McCoy-Wu model and random transverse-field Ising model [16–21]. There must be something missed. We reexamine this problem through studying the difference saddle point equation. The results show that there exist many excited state solutions, which are not found previously. We show that the discreteness in the saddle point solutions plays an important role and the saddle point solutions can not be extended to the continuous limit directly. This can explain the failure of the conventional field-theoretic description simply.

On the other hand, although the strong-disorder renormalization group for the random transverse-field Ising model is very successful [7,8], we hope to provide an angle to understand the McCoy-Wu model. Moreover, in the field theories on the quantum phase transition in many disordered systems, the

*wuxt@bnu.edu.cn

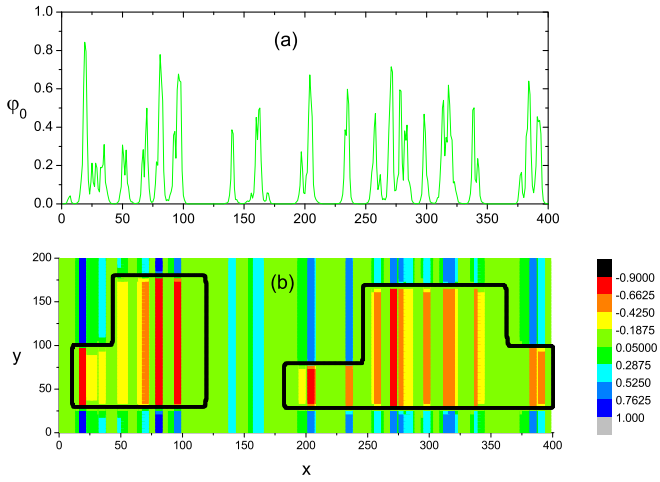

FIG. 1. (a) The ground state saddle point solution. (b) The color map is a typical excited saddle point solution and the black lines are its domain wall. In (a), (b) the temperatures are the same. These solutions are obtained with a random temperature with a uniform distribution.

saddle point equation is the starting point [22]. So, it is very important to understand the saddle point solution. Although there are a lot of qualitative discussions on it, for example, the locally ordered region and replica symmetry breaking [23], the quantitative studies, say numerical calculations, are still rare. The author has carried out numerical calculations to the saddle point equation for the classical phase transition in the disordered systems where the random temperature is short-range correlated [24,25]. In the present problem, the random temperature is strongly correlated in the vertical direction.

In the Landau-Ginzburg-Wilson (LGW) Hamiltonian for the McCoy-Wu model, the reduced temperature is random and only depends on the horizontal coordinate. It does not depend on the vertical coordinate because the McCoy-Wu model is translation invariant in the vertical direction. We solve the saddle point solution of the Landau-Ginzburg-Wilson Hamiltonian numerically. Figure 1 shows the ground state solution and a typical excited state solution for a given random temperature.

As shown in Fig. 1(a), the ground state solution has many peaks and valleys. The ground state solution does not depend on the vertical coordinate and it is the same in each column. At the peaks the solutions are relatively large and at the valleys the solutions are almost zero. The regions at the peaks are locally ordered. We call them locally ordered regions (LORs). These LORs are strips which are infinitely long in the vertical y direction. Because these LORs are one dimensional, they still cannot undergo the phase transition independently. In the saddle point solution, this can be fulfilled with the many excited state solutions, one of which is shown in Fig. 1(b).

As shown in Fig. 1(b), the excited state solution is still striplike. However, it changes the sign in some regions. So, there are domain walls (DWs), where the solution is zero, separating the regions with positive sign and negative sign. The DWs usually consist of broken lines with segments in the x and y directions. The vertical DWs locate at the deep valleys in the ground state solution. For example, there is a vertical DW segment at about $x = 120$, where it is a deep valley in the ground state solution shown in Fig. 1(a). The vertical DW causes a free-energy increase and hence a tension. The horizontal DWs cross the striplike LOR. We find that there is a discreteness free-energy barrier for a horizontal DW. In the excited state solutions, the discreteness barriers are high enough to overcome the tensions caused by the vertical DWs. Then, the horizontal DWs are stable. For example, for the horizontal DW at $45 < x < 120$, $y = 180$ in Fig. 1(b), the discreteness barrier is high enough to overcome the tensions caused by the vertical DWs at $x = 45$ and 120. If the discreteness barrier is not strong enough, the horizontal DW can not be stable. The discreteness barrier plays a key role in the excited state solutions.

The existence of horizontal DW is the reason why the striplike LOR can not undergo phase transition independently. If the mapping to the one-dimensional transverse-field Ising model is considered, the vertical direction is virtual time direction and the horizontal DWs represent the quantum fluctuations.

In the ground state solution, every peak is a LOR. However, not all horizontal DWs across single LOR can be stable. Usually, a stable horizontal DW crosses multiple LORs. Such multiple LORs form an elementary cluster. The criterion for multiple LORs forming an elementary cluster is obtained. We apply the criterion to the saddle point solution with random temperatures distributed uniformly with certain width. Three distribution widths $w = 0.5, 0.4, 0.3$ of random temperature are studied. Taking the excited state solutions into account, the partition function on the saddle point level is an Ising model, in which the elementary clusters behave like superspins. However, the effective Ising model is extremely anisotropic. The horizontal bonds between the elementary clusters are very weak while the vertical bonds are very strong. Both of them are distributed widely. In certain range of temperature in the disordered phase, the system can be dealt as a group of isolated clusters, each of which is an Ising chain in vertical direction. The size distribution of clusters is exponential, hence, the vertical bonds distribution is also exponential.

There is an exponentially small probability of existing elementary clusters (ECs) with extremely large size. These ECs are the so-called rare regions [1]. Then, even if the system is dealt as isolated Ising chains in vertical direction, the susceptibility is divergent in a range of temperature. The rare regions, the ECs with extremely large size, are responsible for the divergence. The Griffiths-McCoy singularity can be explained.

We have also studied the saddle point solutions for the random temperature with the binary probability distribution. It is found that the size and vertical bond distribution are still exponential in certain range of temperature. In other words, the Griffiths-McCoy singularity in the saddle point solutions does not depend on the distribution of random temperature.

The paper is arranged as follows. In Sec. II, the Landau-Ginzburg-Wilson Hamiltonian for McCoy-Wu Ising model is given. In Sec. III, the discreteness barrier in the difference saddle point equation is shown. In Sec. IV, the stable condition for the horizontal DW across a single LOR is studied. In Sec. VI, the criterion for an elementary cluster formed with multiple LORs is given. In Sec. VII, the saddle point solutions with random temperature distributed uniformly and binarily are obtained. The Griffiths-McCoy singularity is discussed. Section VII is a summary.

II. LGW HAMILTONIAN

For convenience, we rotate the original McCoy-Wu Ising model 90°, the horizontal couplings are random from column to column and identical in each column, the vertical couplings are the same. Then, in the vertical direction, the system is translation invariant. Using the Stratonovich-Hubbard transformation, we map McCoy-Wu model to a Landau-Ginzburg-Wilson Hamiltonian on the square lattice (see the detail in Appendix):

$$H = \sum_{i,j}\left\{\frac{1}{2z}[(\phi_{i+1,j}-\phi_{i,j})^2+(\phi_{i,j+1}-\phi_{i,j})^2] + \frac{t_i}{2}\phi_{i,j}^2+\frac{g}{4}\phi_{i,j}^4-\beta_C h\phi_{i,j}\right\}, \tag{1}$$

where $\phi_{i,j}$ is the order parameter and i,j are the horizontal and vertical coordinate of lattice site; $z=4$ is the coordinate number on the square lattice. For the Ising model, it has $g=\frac{1}{3}$. The random temperature t_i depends only on the horizontal coordinate. $\beta_C = 1/(zJ)$ is the inverse of critical temperature and J is the average coupling.

The reduced temperature t_i depends only on the horizontal coordinate since in the vertical direction the system is translation invariant. We can write

$$t_i = t_0 + \delta t_i, \tag{2}$$

where t_0 is average reduced temperature and δt_i is the random part. The distribution of δt_i is related to the distribution of the random couplings in the McCoy-Wu Ising model.

For convenience, we introduce the transformations

$$\varphi_{i,j} = \sqrt{zg}\phi_{i,j},\ t_i' = zt_i,\ \ h' = \sqrt{gz^3}\beta_C h \tag{3}$$

and we get

$$H = \frac{1}{gz^2}\sum_{i,j}\left\{\frac{1}{2}[(\varphi_{i+1,j}-\varphi_{i,j})^2+(\varphi_{i,j+1}-\varphi_{i,j})^2] + \frac{t_i'}{2}\varphi_{i,j}^2+\frac{1}{4}\varphi_{i,j}^4-h'\varphi_{i,j}\right\}. \tag{4}$$

The saddle point equation for the above Hamiltonian is given by

$$-(\varphi_{i+1,j}+\phi_{i-1,j}+\varphi_{i,j+1}+\varphi_{i,j-1}-4\varphi_{i,j}) + t_i'\varphi_{i,j}+\varphi_{i,j}^3-h'=0. \tag{5}$$

Note that it is a discrete difference equation. The transformed temperature is $z=4$ times of the original temperature. Therefore, the transformed temperature distribution width is also multiplied by $z=4$.

There exist many excited state solutions for the saddle point equation. If $\underline{\varphi}_{i,j}$ is a solution of Eq. (5), its free energy is given by

$$F(\{\underline{\varphi}_{i,j}\}) = -\frac{1}{gz^2}\sum_{i,j}\left(\frac{1}{4}\underline{\varphi}_{i,j}^4+\frac{1}{2}h'\underline{\varphi}_{i,j}\right). \tag{6}$$

We use the "underline" to denote the excited state solution. The above equation is obtained by substituting Eq. (5) into Eq. (4), and dealing h' as a perturbation since we only concern the case $h'\to 0$ for the critical phenomena.

At the saddle point level, where the fluctuation around the saddle point solution is neglected, the partition function is given by

$$Z_{\rm sad} = \sum_\alpha e^{-F_\alpha}, \tag{7}$$

where the summation is carried out over all the excited state solutions.

It should be pointed out that the discreteness plays a key role in the present problem. Therefore, we shall keep the discrete form throughout the paper. In addition, we have a convention about the denotation of coordinates. We use i (or j) to denote x coordinate (or y coordinate) when it is an integer.

If it has $|t|\ll 1$, one can get the continuum limit of Eq. (1). It turns into the well-known continuous Landau-Ginzburg-Wilson Hamiltonian in which the coordinates i,j are replaced by continuous coordinates x,y and the lattice constant is set to be the unit length. Correspondingly, the saddle point equation becomes

$$-\left(\frac{\partial^2\varphi}{\partial x^2}+\frac{\partial^2\varphi}{\partial y^2}\right)+t'(\mathbf{r})\varphi+\varphi^3+h'=0. \tag{8}$$

We call it continuous saddle point solution.

III. KINK SOLUTION WITH A CONSTANT TEMPERATURE

A. Continuum limit

It is known early that there are excited state solutions even for the pure system [26], that is, the kink solution. As we know, the kink solution is obtained in the continuum limit. The discreteness of lattice should induce something different from the continuum limit solution. In the previous studies, these differences are ignored generally because it is believed that they are not important. This is correct in the critical phenomena in the pure system since the correlation length approaches to infinity in the asymptotic regime and then the detail of lattice becomes unimportant. However, we will see that the discreteness plays a key role in the present disordered system.

We start from the continuum limit solution, which can be a benchmark for our numerical solution. In a pure two-dimensional system, the temperature in Eq. (8), the reduced temperature t, is a constant. Assuming variation in only y direction and without the external field, Eq. (8) becomes

$$-\frac{d^2\varphi}{dy^2}+t\varphi+\varphi^3=0, \tag{9}$$

where t is a constant. If $t<0$, aside from the ground state solution $\varphi_0=\pm\sqrt{-t}$, there are excited state solutions [26]

$$\underline{\varphi}(y) = \pm\sqrt{-t}\tanh\sqrt{\frac{-t}{2}}y. \tag{10}$$

We use the "underline" to denote the excited state solution. For these excited state solutions, there are two phases separated by an interface, where $\varphi(y)=0$. The interface is the domain wall (DW). Here, the DW is a straight line. The free energy of excited state solution is higher than that of ground sate. We call their difference the free-energy increase. Substituting the above solution into the Hamiltonian, one gets the free-energy

increase per unit length of DW. It is given by

$$f_d = \frac{2\sqrt{2}}{3gz^2}(-t)^{3/2}. \tag{11}$$

Because the DW is infinitely long and its free-energy increase is infinitely large, the kink solution does not play an important role in critical phenomena in the pure systems.

We can show this solution is marginally stable under perturbation. To study the stability of the kink solution, we consider the fluctuation near it. Let

$$\tilde{\varphi} = \varphi - \underline{\varphi} \tag{12}$$

and consider the Gaussian approximation of the continuous Landau-Ginzburg-Wilson Hamiltonian for this fluctuation:

$$\delta H = \frac{1}{gz^2}\int dx\,dy\left\{\frac{1}{2}\left(\frac{\partial\tilde{\varphi}}{\partial x}\right)^2 + \left(\frac{\partial\tilde{\varphi}}{\partial y}\right)^2 + \frac{1}{2}[t + 3\underline{\varphi}^2]\tilde{\varphi}^2\right\}. \tag{13}$$

The eigenmodes of $\tilde{\varphi}$ satisfy the following equation:

$$-\left(\frac{\partial^2\tilde{\varphi}}{\partial x^2} + \frac{\partial^2\tilde{\varphi}}{\partial y^2}\right) + [t + 3\underline{\varphi}^2]\tilde{\varphi} = \lambda\tilde{\varphi}. \tag{14}$$

For the eigenmode with the lowest eigenvalue, the fluctuation in the x direction must be zero in the above equation. Differentiating Eq. (9) with respect to y, it is easily shown that

$$\dot{\underline{\varphi}} = \frac{d\underline{\varphi}}{dy} = \pm\frac{|t|/\sqrt{2}}{\cosh^2(\sqrt{-t/2}y)} \tag{15}$$

is an eigenmode and its eigenvalue is zero. In fact, this eigenmode is just a global translation of the kink. Since the system is continuously translation invariant, such a translation causes no free-energy increase. This mode is marginal with respect to the perturbation. The eigenvalues of other modes are larger than zero and they are stable. This can be verified by numerical method.

B. Discreteness barrier

Now, we consider the pure system on a lattice, where the reduced temperature is a constant on the lattice. Assuming variation in only vertical direction, the discrete saddle point equation (5) becomes

$$-(\varphi_{j+1} + \varphi_{j-1} - 2\varphi_j) + t\varphi_j + \varphi_j^3 = 0, \tag{16}$$

where it reduces to be one dimensional. This equation can be solved by a simple iteration algorithm

$$\varphi_j^{(n+1)} = \omega\varphi_j^{(n)} + \frac{(1-\omega)}{2}\left[\varphi_{j+1}^{(n)} + \varphi_{j-1}^{(n)} - t\varphi_j^{(n)} - \left(\varphi_j^{(n)}\right)^3\right], \tag{17}$$

where ω is the relaxing parameter. We denote the converged solution with a domain wall by $\underline{\varphi}_j$. Its free energy is given by

$$F = -\frac{1}{4gz^2}\sum_j \underline{\varphi}_j^4. \tag{18}$$

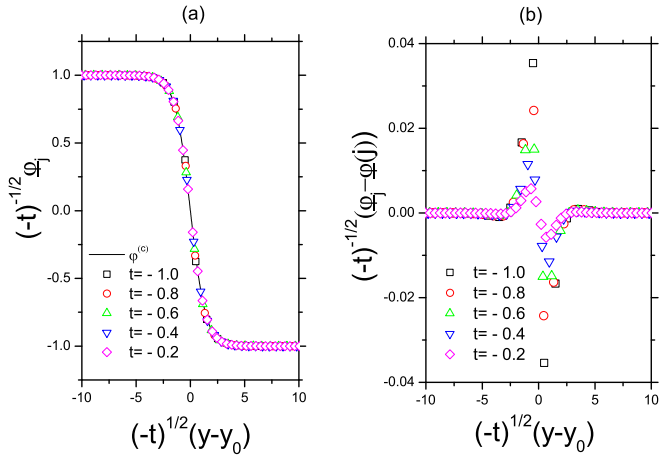

FIG. 2. (a) The discrete kink solutions on a lattice. The solid line is the continuous kink solution. (b) The differences between the discrete and the continuous kink solution.

It can be expected that the solutions for the continuous and discrete saddle point solution are approximately equal. The solutions with several temperatures are shown in Fig. 2. In Fig. 2(a), the rescaled solutions with temperature $t = -1.0, -0.8, -0.6, -0.4, -0.2$ coincide with the continuous solution [Eq. (10)]. However, there are differences between the discrete solution and the continuous ones. In Fig. 2(b) these differences are shown. The differences are small indeed even for $t = -1.0$ and become smaller and smaller as $|t|$ decreases.

All the discrete solutions are obtained on a lattice with length $L = 300$. The open boundary condition is used. We set the initial value of φ to be $\varphi_j^{(0)} = 1$ for $-149 \leqslant j \leqslant 0$ and $\varphi_j^{(0)} = -1$ for $0 < j \leqslant 150$. The DW in the converged solution locates between the site of $j = 0$ and 1. Simply interpolating we get that the DW location is $y_0 = 0.5$. This is the value of y_0 in Fig. 2.

All the converged solutions show that the DW locates just at the middle of the neighbored rows, i.e., $y_0 = n + 0.5$ where n is an integer. We will show that this solution is stable in two ways. First, we analyze the stability with respect to the fluctuation. Let

$$\tilde{\varphi}_j = \varphi_j - \underline{\varphi}_j, \tag{19}$$

where $\underline{\varphi}_j$ is the converged solution with a kink. We consider the Gaussian approximation of Landau-Ginzburg-Wilson Hamiltonian (4) for the this fluctuation:

$$\delta H = \frac{1}{gz^2}\sum_j\left\{\frac{1}{2}(\tilde{\varphi}_j - \tilde{\varphi}_{j-1})^2 + \frac{1}{2}[t + 3(\underline{\varphi}_j)^2]\tilde{\varphi}_j^2\right\}, \tag{20}$$

where the variation in horizontal direction is ignored. The eigenmodes of $\tilde{\varphi}$ satisfy the following equation:

$$-(\tilde{\varphi}_{j+1} + \tilde{\varphi}_{j-1} - 2\tilde{\varphi}_j) + \left[t + 3\underline{\varphi}_j^2\right]\tilde{\varphi}_j = \lambda\tilde{\varphi}_j. \tag{21}$$

We solve this eigenequation with LAPACK. It is found that all the eigenvalues are positive. The lowest smallest eigenvalues λ_1 for different t are shown in Fig. 3.

In Fig. 3(a), we show typical first eigenmode of Eq. (15), which has the lowest eigenvalue λ_1. They can be approximated

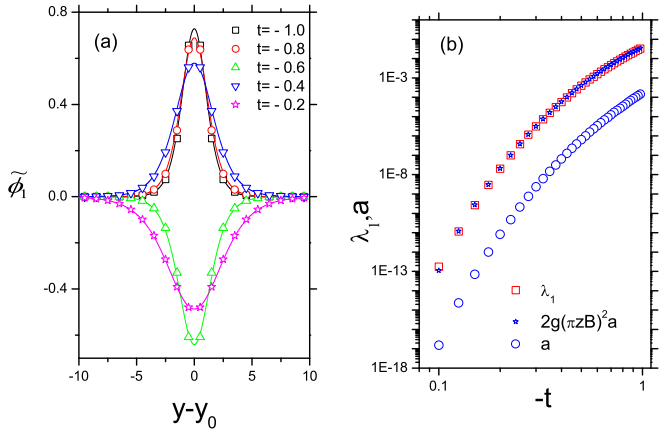

FIG. 3. (a) The first eigenmodes of Eq. (21). The solid lines are the continuous eigenmodes given by Eq. (15). (b) The first eigenvalue λ_1 and the discreteness barrier a vs the temperature t. Equation (26) shows that $\lambda_1 \approx 2gz^2(\pi B)^2 a$.

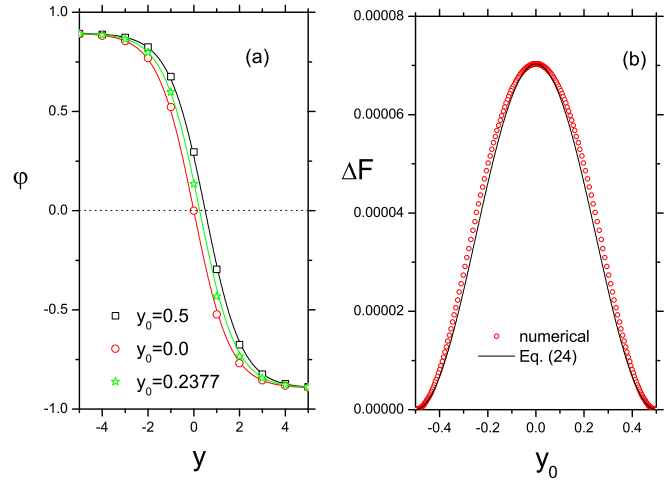

FIG. 4. (a) Three transient states φ_j with different DW locations. The scatters are obtained from numerical solution of Eq. (17) during the iteration. The solid lines are obtained from the continuous functions $\underline{\varphi}(y - y_0)$. In order to see the DW location y_0, a dotted line for $\varphi = 0$ is drawn. (b) The free-energy increases of the transient states vs the DW locations.

by Eq. (10) since they are the continuous counterparts. As mentioned after Eq. (15), this eigenmode is just a globe translation of the kink. However, on the lattice there is only discrete translation invariance rather than the continuous one. Although the first eigenvalues of Eq. (15) are very small, they are positive and not equal to zero. This means that the discrete kink solutions are stable!

Second, to understand the stability of the discrete kink solution, we study the transient states during the iteration of Eq. (17). In Fig. 3(a), three states are shown for $t = -0.8$. The state shown with black square is the converged solution $\underline{\varphi}_j$, which is stable. The states shown with red and green scatters are transient states. These states can be approximated by the continuous kink solution

$$\varphi_j \approx \underline{\varphi}(j - y_0), \tag{22}$$

where $\underline{\varphi}(y)$ is the kink solution defined by Eq. (10) and y_0 is the location of DW, which is obtained by interpolation in the numerical calculation. In Fig. 3(a), to show the location of the domain wall, a dotted straight line is drawn for $\varphi = 0$. The solid curves are the continuous functions $\underline{\varphi}(y - y_0)$.

The solution with $y_0 = 0$ [the red circle in Fig. 4(a)] is obtained by setting the initial condition as $\varphi_j^{(0)} = 1$, for $-L < j < 0$, $\varphi_0^{(0)} = 0$, and $\varphi_j^{(0)} = -1$, for $0 < j < L$. The length of lattice is $2L + 1$. The antisymmetry about $j = 0$ in the initial condition is kept in the iteration, so the solution should converge to such a solution with $y_0 = 0$. But, it is unstable with respect to perturbation, for example, if we set the initial value $\varphi_0^{(0)} = 0.000\,01$ at $j = 0$ (or $\varphi_0^{(0)} = -0.000\,01$). It will converge slowly to the solution with $y_0 = 0.5$ (or $y_0 = -0.5$), which is stable. The iteration process is as follows. After some steps, the transient states converge to kink shape. Then, the kink shape stays the same, but the location of DW shifts. During the iteration, we record the transient states after every 500 times of iteration, then we get the data in Fig. 4(b). For each recorded transient state we calculate its free energy F defined in Eq. (18). The free-energy increase is defined by

$$\Delta F = F - F_d, \tag{23}$$

where F_d is the free energy of the solutions with $y_0 = \pm 0.5$. We recorded many transient states, of which free-energy increases are shown in Fig. 4(b). Considering the discrete lattice translation symmetry, the free-energy increase should be a periodic function on y_0 with period 1. The curve in Fig. 4(b) is just a period for y_0 from -0.5 to 0.5.

It can be seen that the relation between the free-energy increase and the location of DW is approximately given by

$$\Delta F = \frac{a}{2}[\cos(2\pi y_0) + 1]. \tag{24}$$

In Fig. 4(b), the black solid line is drawn from the above equation with $a = 7.0323 \times 10^{-5}$. From this equation, we can see that there is a free-energy barrier as the location of DW shifts. The height, from the lowest to the highest free energy, is a. We call a the discreteness barrier. For different t, the discreteness barriers a are calculated numerically and shown in Fig. 3(b).

Just due to this discreteness barrier, the stable DW can only locate in the middle of two neighbored rows. Of course, for a pure system, the DW length is infinite long and induces an infinitely large free-energy increase. So, it does not play an important role. However, for inhomogeneous and random systems, the DW length can be finite. Then, the discreteness barrier will play a key role.

We find that the discreteness barrier a is related to the eigenvalue λ_1 of the first eigenmode in a simple way. The first eigenmode in Fig. 2(a) is with respect to the stable state with $y_0 = n + 0.5$ where n is an integer. It is approximately given by

$$\tilde{\varphi}_{1j} \approx B\dot{\underline{\varphi}}(j - y_0), \tag{25}$$

where $\dot{\underline{\varphi}}(y)$ is defined in Eq. (15) and $B^2 = 2\sqrt{2}|t|^{3/2}/3$ is the normalization constant.

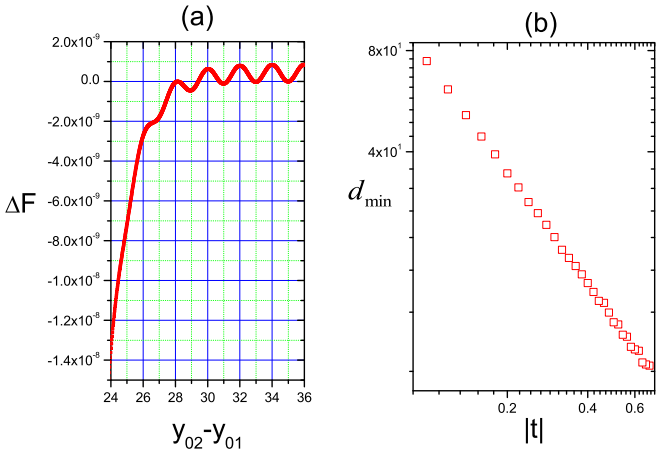

FIG. 5. (a) The free-energy increases vs the distance between the domain walls for $t = -0.25$. (b) The minimal distance between two domain walls for different temperature.

The transient states with $y_0 = 0.5 + \delta y_0$ near $y_0 = 0.5$ can be regarded as shifting the whole kink a small distance δy_0. Considering the fluctuation proportional to the first eignemode, i.e., $\tilde{\phi} = c\tilde{\varphi}_1$, from Eqs. (20) and (21), one gets the free-energy increase caused by this shift $\Delta F = \lambda_1 c^2/2gz^2$. On the other hand, the variation caused the first mode can be approximated by $\tilde{\phi} = \dot{\varphi}^{(c)}\delta y_0$. Then, it has $\delta y_0 = cB$. The free-energy increase due to the shit of DW is $\Delta F = \frac{a}{4}(2\pi)^2(\delta y_0)^2 = \frac{a}{4}(2\pi)^2 c^2 B^2$. Therefore,

$$\lambda_1 \approx 2g(\pi z B)^2 a. \tag{26}$$

As shown in Fig. 3(b), this relation agrees with the numerical results well.

C. Minimal distance between two kinks

Now, we consider two-kink solutions. They are obtained by setting the initial condition as $\varphi_j^{(0)} = -\sqrt{-t}$, for $1 \leqslant j \leqslant n_d$, and $\varphi_j^{(0)} = \sqrt{-t}$, for $n_d \leqslant j \leqslant L$, where L is the length of lattice and the periodic condition is used in the numerical calculation. Then, the solution will converge to a two-kink solution. There are two DWs and we denote their locations by y_{01} and y_{02}, which are obtained from the numerical solution with a simple interpolation. The distance between two DWs is denoted by $d = |y_{02} - y_{01}|$.

Similar to the one-kink solutions, one may record the transient states and their free energy. Figure 5(a) shows their free-energy variation ΔF with the distance between two DWs. The variation ΔF is defined are $\Delta F = \Delta F_2 - 2\delta F_1$, $\Delta F_2 = F_2 - F_g$, and $\Delta F_1 = F_1 - F_g$, where F_2 is the free energy of transient with two kinks; F_1 is the free energy of the stable solution with one kink, F_g is the ground state free energy. The lattice length is 600 and the temperature is $t = -0.25$. As shown in Fig. 5(a), the free energy varies with the distance d as a periodic function for $d > 30$. In this case, the two DWs can be regarded as two isolated DWs. The free energy is locally minimal at $d = 31,33,35\ldots$ since the two DWs locate at the middle of two neighbored sites. These solutions are stable. For $d = 30,32,34,\ldots$, the free energy is locally maximal. For these states, the two DWs locate at the positions with integer coordinate. They are unstable. For $d < 28$, it goes down quickly as the distance d decreases and there is no stable solution. $d = 29$ is minimum distance for a stable two-kink solution.

This example tells us that if two DWs are too close they are unstable. There is a shortest distance between two stable DWs. For different temperatures, the shortest distances of two DWs $d_{\min}$ are calculated. The results are shown in Fig. 5(b). The log-log plot shows a perfect straight line. The fitted result is given by $d_{\min} \approx 5.9|t|^{-1.1}$.

IV. TWO-DIMENSIONAL EXCITED STATE SOLUTIONS

Now, we study the excited state solutions of two-dimensional saddle point equation (5) with an inhomogeneous temperature. With these examples, we show the basic concepts, quantities, and rules. We show that the rules are general. Then, we apply these rules to the random temperature cases.

A. LORs and four quantities to describe them

We consider a system with six regions. The ranges of the regions are $0 < x \leqslant 10$, $110 < x \leqslant 120$ for region 1; $10 < x \leqslant 30$, $30 < x \leqslant 50$, $30 < x \leqslant 50$, $70 < x \leqslant 90$, $90 < x \leqslant 110$ for regions 2, 3, 4, 5, 6, respectively. The temperatures in these regions are set to be 0.4, -0.7, t_3, -0.6, t_5, -0.7, 0.4, respectively. The boundary condition is periodic. We set $t_3, t_5 > 0$ and adjust them to study the stability of the domain wall. In this case, the temperature is correlated in a finite range, 20 lattice constants. However, our conclusions are not dependent of this correlation and based on general analysis.

For the ground state solution, there is no variation in the vertical (y) direction. Then, the saddle point equation (5) without external field for the ground state solution becomes

$$-(\varphi_{i+1,j} + \varphi_{i-1,j} - 2\varphi_{i,j}) + t_i\varphi_{i,j} + \varphi_{i,j}^3 = 0. \tag{27}$$

This equation depends only on the x coordinate rather than y coordinate. Figure 6(a) shows the ground state solution with temperature stated above and $t_3 = t_5 = 0.1$. In regions 2,4,6, the reduced temperature is negative, so the solution is nonzero. In regions 1,3,5, the reduced temperature is positive, so the solution decays to be very small and close to zero.

There are three peaks in the ground state solution. The regions of the three peaks are locally ordered. We call them locally ordered regions (LORs). In Fig. 6(a), three LORs are labeled by words in blue. We determine the spatial range of the LOR by the minimum. One can see that the ranges of three LORs are $0 < x < 40$, $40 < x < 80$, and $80 < x < 120$, respectively. We call these ranges the sizes of LOR. Here, the sizes of the three LORs are the same $l_n = 40$.

As shown in Fig. 1, in the excited state solutions, there are vertical DWs, which locate between neighbored LORs. To calculate the free-energy increase due to such a DW between two neighbored LORs, we separate the two LORs off the system. For example, as shown in Fig. 6(b), we separate LORs 1,2 off. The temperatures are set to be the same, but we only consider part of the system for $0 < x \leqslant 80$, in which the saddle point equation (27) is solved with open boundary condition.

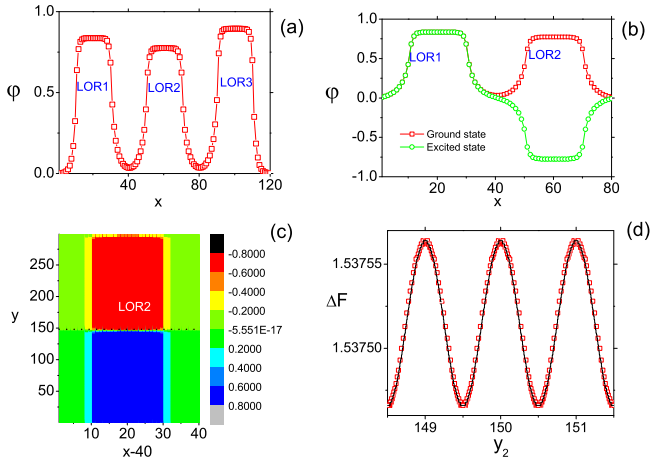

FIG. 6. (a) The ground state solution for the temperature stated in the text. There are three peaks. We call them three LORs. (b) The ground state and excited state solutions for the calculation of the coupling between LORs 1 and 2. Here, $t_2 = t_4 = 0.1$. (c) The excited state solutions for the calculation of the discreteness barrier of the domain wall across LOR 2. The color map is the solution and the black dotted line is the DW. (d) The free-energy increase as the location of DW shown in (c) varies.

The ground state solution and excited state solution are shown in Fig 6(b). The open boundary condition guarantees that there is only one DW between LORs 1 and 2. For any two neighbored LORs, we can carry out this calculation. Consider such a DW crosses the whole system along the y direction. Let the free-energy increase per unit length due to this DW be

$$2k^x_{n,n+1} = F^E_{n,n+1} - F^G_{n,n+1}, \tag{28}$$

where $F^G_{n,n+1}, F^E_{n,n+1}$ are the free energy of the ground state and excited state solution of Eq. (27) for nth and $(n+1)$th LORs, respectively. The significance of $2k^x_{n,n+1}$ is discussed later. The free energy is obtained with $F = -\frac{1}{gz^2}\sum_i \frac{\varphi^4_{i,j}}{4}$. In principle, one should calculate this free-energy increase taking the whole system into account. However, the solution near the DW between LORs 1 and 2 is only related to LORs 1,2 closely and not influenced much by the remote part like LOR 3. Moreover, this method can save computing time.

To study the DW across a LOR, for example, LOR 2, we can study LOR 2 separately. We separate LOR 2 off by solving the two-dimensional saddle point equation (5) only for $40 < x < 80$. We use open boundary conditions in both directions. There exist stable excited state solution with a DW across the LOR as shown in Fig. 6(c). The black dotted line is the DW. For any LOR, we can calculate the free-energy increase due this kind of DW. Let it be

$$2k^y_n = F^E_n - F^G_n, \tag{29}$$

where F^E_n, F^G_n are the free energies for the excited state with a DW across the nth LOR and ground state solution, respectively. The significance of $2k^y_n$ is discussed later.

To show the stability of this solution, we study the free energy of transient state. By tuning the initial values as in Sec. III, we can get the transient states. In Fig. 6(d), we show the free energy of transient state with a DW across LOR 2 shown in Fig. 6(c). We characterize the transient state with the location of DW y_2, where the SP solution is zero. For $y_2 = 149.5, 150.5, 151.5, \ldots$, the free energy is locally minimal and its value is about 1.5375. In the converged solutions, the DW just locates at $y_2 = 149.5, 150.5, 151.5, \ldots$. The free energy is a periodic function of y_2 with period 1. The data in Fig. 6(d) are obtained piece by piece. For example, if we set the $y_0 = 149.001$ initially, the solution will converge to $y_0 = 149.5$ and if we set $y_0 = 148.999$ initially, the solution will converge to $y_0 = 148.5$.

The free energy of the transient state as shown in Fig. 6(d) should be approximately

$$\Delta F_n = 2k^y_n + \frac{a_n}{2}[\cos(2\pi y_n) + 1] \tag{30}$$

for nth LOR, where $\Delta F_n = F^E_n - F^G_n$, F^E_n is the free energy of the transient state, and F^G_n is that of the ground state. $2k^y_n$ is the free-energy increase of DW across LOR n. The discreteness barrier, which equals to the height from lowest free energy to the highest free energy, is a_n. In Fig. 6(d), it has $2k^y_2 = 1.5375$ and $a_2 = 9.7385 \times 10^{-5}$.

This discreteness barrier is the counterpart of that obtained in Sec. III, where the temperature is a constant. It depends on the temperature in the LOR. Generally speaking, it can be influenced by the neighbored LOR, but this kind of influence must be very small. Since the saddle point solution, especially at the peak, is mainly determined by the local temperature. Therefore, we can separate the LORs off and study the discreteness barrier individually.

It costs too much computing time to extract the discreteness barrier a_n according to the above discussion. We have a simpler algorithm, in which only two solutions are solved. One is obtained by setting the initial DW at the center of the system, i.e., $\varphi^{(0)}_{i,j} = -1$ for $-L \leqslant i < 0$, $\varphi^{(0)}_{i,0} = 0$, and $\varphi^{(0)}_{i,j} = 1$ for $0 < j \leqslant L$. Because during the iteration the antisymmetry in the solution is kept, the DW in the converged solution is at $j = 0$. This solution is unstable with respect to perturbation. Another one is obtained by setting the initial DW between two neighbored rows, i.e., $\varphi^{(0)}_{i,j} = -1$ for $-L \leqslant i < 0$, and $\varphi^{(0)}_{i,j} = 1$ for $0 \leqslant j \leqslant L$. The converged solution is stable. The free-energy difference of these two solutions is the discreteness barrier a_n.

For a LOR, we need four quantities: the size l_n, the coupling in x direction $k^x_{n,n+1}$, in y direction k^y_n, the discreteness barrier a_n. For any LOR we can calculate them according to the above algorithms.

B. Two basic shapes of DW segments

Figures 7(a) and 7(b) show typical stable excited state solutions of Eq. (5) for the temperatures stated in the last subsection. The colored map shows the excited state solutions. The domain walls, where the solution changes sign, are shown with black lines. They are approximately composed of horizontal and vertical segments. As we discussed above, there are three LORs, which are labeled by words in white. The vertical DW segments locate just at the borders between two neighbored LORs and the horizontal DW segments cross the LORs.

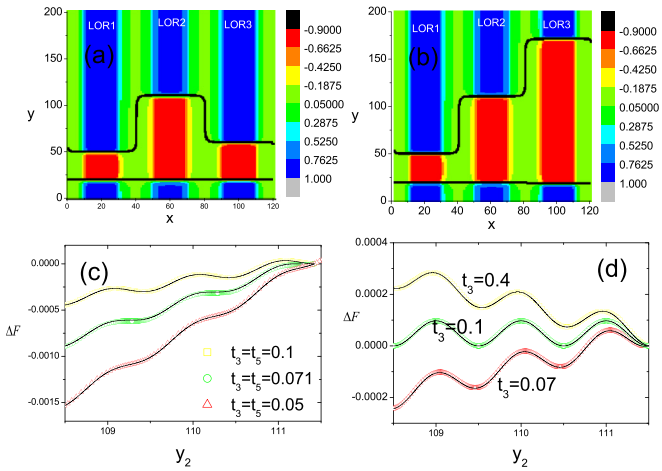

FIG. 7. Basic shapes of DWs. In (a) and (b) the color maps are the saddle point solutions and the black lines are DWs. (a) The DW segment across LOR 2 and the two DW segments it connects form a shape of a "big cap." (b) The DW segment across LOR 2 and the two DW segments it connects form a shape of an "elbow." (c) The free-energy variation of the transient states vs y_{02}, the location of DW across LOR 2 with big cap DW segments as shown in (a). (d) The free-energy variation of the transient states vs y_{02}, the location of DW across LOR 2 with elbow DW segments as shown in (b).

Figures 7(a) and 7(b) show two basic shapes for the horizontal DW segments and vertical DW segments. See the horizontal DW segment at $40 < i < 80$, $j = 110$. It connects with two vertical DW segments, one is between LOR 2 and LOR 1, and another one is between LOR 2 and LOR 3. The three segments in Fig. 7(a) form a shape of "big cap" and in Fig. 7(b) form a shape of an "elbow."

The free energy depends on the positions of the DWs obviously. We show the free energy of the transient states in Fig. 7(c) for the big cap case shown in Fig. 7(a). We adjust the initial condition and record the transient states. The position of the upper DW across the LOR 2 is labeled by y_2. In the numerical calculation, y_2 is obtained by simple interpolation at the middle of the LOR 2, i.e., $x = 60$. In the three cases with $t_3 = t_5 = 0.1, 0.071, 0.05$ in Fig. 7(c), only the upper DW across LOR 2 is moving in the iterations. Therefore, the free energy of transient states only depends on y_2. We find that the free energy of the transient states can be approximately given by

$$\Delta F \approx 2\left(k^x_{1,2} + k^x_{2,3}\right) y_2 + \frac{a_2}{2}\cos(2\pi y_2) + C, \tag{31}$$

where C is constant to make $\Delta F = 0$ at a reference point, whose position is $y_0 = 111.5$. The length of the segment of DW between LORs 1 and 2 increases with y_2. As discussed above, $2k^x_{12}$ is the free-energy increase per unit length of DW between LORs 1 and 2. $2k^x_{23}$ is that between LORs 2 and 3. That between LORs 2 and 3 also increases with y_2. The third term stems from free-energy variation due to the horizontal DW across LOR 2 defined in Eq. (30). a_2 is discreteness barrier of LOR 2. The three parameters $2k^x_{12}, 2k^x_{23}, a_2$ are calculated according to the algorithm in the last subsection. They are given in Table I.

TABLE I. The parameters for the curves in Fig. 7.

t_3	t_5	$2k^x_{12}$	$2k^x_{23}$	a_2
0.1	0.1	7.517×10^{-5}	7.517×10^{-5}	9.741×10^{-5}
0.071	0.071	1.525×10^{-4}	1.525×10^{-4}	9.793×10^{-5}
0.05	0.05	2.612×10^{-4}	2.612×10^{-4}	9.836×10^{-5}
0.4	0.1	3.308×10^{-7}	7.517×10^{-5}	9.564×10^{-5}
0.1	0.1	7.517×10^{-5}	7.517×10^{-5}	9.741×10^{-5}
0.07	0.1	1.564×10^{-4}	7.517×10^{-5}	9.769×10^{-5}

We choose three cases $t_3 = 0.4, 0.1, 0.07$ for the elbow shape shown in Fig. 7(b) to show the free-energy variation with y_2 in Fig. 7(d). In all three cases, it has $t_5 = 0.1$. The relation between the free energy and the location of the DW across LOR 2 can be approximately given by

$$\Delta F \approx 2\left(k^x_{1,2} - k^x_{2,3}\right) y_2 + \frac{a_2}{2}\cos(2\pi y_2) + C, \tag{32}$$

where C is constant to make $\Delta F = 0$ at a reference point, whose position is $y_0 = 111.5$. Similarly, $2k^x_{12}$ is the free-energy increase per unit length of DW between LORs 1 and 2. $2k^x_{23}$ is that between LORs 2 and 3. The length of the vertical DW between LORs 1 and 2 increases with y_2. That between LORs 2 and 3 decreases with y_2.

It can be easily seen that the formula for the big cap is valid for the "big cup" case and the formula for elbow is still valid if the elbow is reversed. In addition, the above two formulas are valid only for $|y_2 - y_3| \gg 1$ and $|y_2 - y_1| \gg 1$, where y_1, y_3 are the y coordinates of the upper DW across the LORs 1 and 3, respectively.

The scatters in Figs. 7(c) and 7(d) are the numerical results of the free energy of the transient states and the solid curves are obtained from Eqs. (32) and (31) with parameters give in Table I. The agreement between the numerical results and Eqs. (32) and (31) are good.

The DW segment across LOR 2 is stable if the free energy is locally minimal. In Fig. 7(c), for $t_3 = t_5 = 0.1$ it is stable at about $y_2 = 109.5, 110.5$. For $t_3 = t_5 = 0.071$, it is marginally stable at $y_2 = 109.5, 110.5$, where the second derivative of free energy with respect to y_2 is zero. For $t_3 = t_5 = 0.05$, it is unstable in Fig. 7(c). In Fig. 7(d), in the three cases, one can see the DW segment across LOR 2 is stable at about $y_2 = 109.5, 110.5$, where the free energy is locally minimal.

Figuratively speaking, the vertical DWs between LORs cause tensions and the horizontal DWs across the LORs cause resistances stemming from the discreteness barrier. In the next subsection, we discuss the stability condition for the DW segment across LOR.

C. Generalized force and the stable condition for the horizontal DW

Combining Eqs. (32) and (31), we assume the free-energy increase concerning the elbow and big cap as shown in Figs. 7(a) and 7(b) in a unified form

$$F = \mathfrak{F}_{1,2} + \mathfrak{F}_{2,3} + \mathfrak{G}_2, \tag{33}$$

where the first two terms stem from the vertical DWs between LORs 1 and 2 and between 2 and 3; the third term stems from

the horizontal DW across LOR 2. The first two terms can be written generally

$$\mathfrak{F}_{n,n\pm1} = \mathfrak{F}_{n,n\pm1}(|y_n - y_{n\pm1}|). \tag{34}$$

Here, $n = 2$ and y_1 and y_3 are the y coordinates of the upper horizontal DWs across the LORs 1 and 3, respectively. The third term can be written generally

$$\mathfrak{G}_n \approx \frac{a_n}{2}\cos(2\pi y_n) \tag{35}$$

because the DW across the LOR n has a discreteness barrier with amplitude a_n. Then, we can introduce three generalized forces

$$\tau_{n\pm1,n} = -\frac{\partial \mathfrak{F}_{n,n\pm1}}{\partial y_n} \tag{36}$$

and

$$\rho_n = -\frac{\partial \mathfrak{G}_n}{\partial y_n}. \tag{37}$$

Obviously, $\tau_{1,2}$ ($\tau_{3,2}$) are the tensions from the vertical DW between LORs 1 and 2 (LORs 2 and 3); ρ_2 is the resistance of the horizontal DW across LOR 2 due to the discreteness barrier.

To show the generalized force in detail, we consider the big cap case shown in Fig. 7(a). We set $y_1 = 50.5$, $y_3 = 120.5$ and $t_1 = 0.4$, $t_2 = -0.7$, $t_3 = 1.0$, $t_5 = 0.07$, $t_6 = -0.7$. We only change t_4 and we show four cases with $t_4 = -0.3, -0.4, -0.5, -0.54$ in Fig. 8.

In the numerical calculation, we calculate the net generalized force with difference method. After we get the free energy of the transient states, we calculate differentiation of F respect to y_2 to get the net force. Because of $t_3 = 1.0$, the free-energy increase due to the vertical DW between LORs 1 and 2 is so small that the tension $\tau_{1,2} \approx 2k_{1,2} \sim 10^{-9}$ can be omitted. Therefore, the tension $\tau_{2,3}$ and the resistance ρ_2 dominate.

For all the four cases in Fig. 8, there are two common features. The first one is that the generalized force $-\frac{\partial F}{\partial y_2}$ has an oscillating part with oscillation period 1. The second one

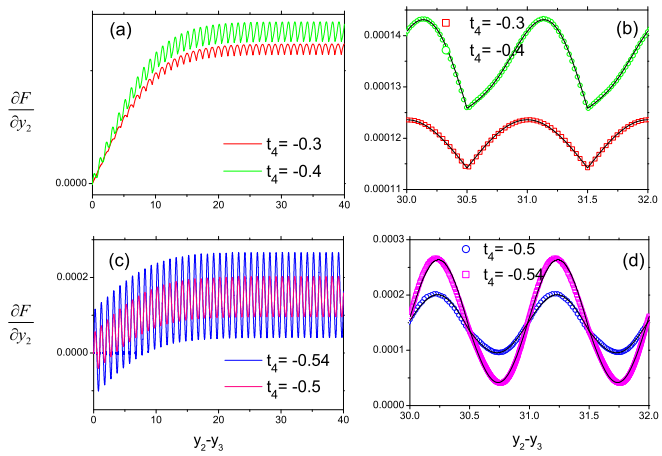

FIG. 8. (a) The net generalized force with $t_4 = -0.3, -0.4$. (b) The fine structure of the generalized forces in (a) for $y_{02} - y_{03} \gg 1$. (c) The net generalized force with $t_4 = -0.5, 0.54$. (d) The fine structure of the generalized forces in (c) for $y_2 - y_3 \gg 1$.

is that the oscillation center, which is obtained by averaging the oscillating part in a period, approaches zero with $|y_2 - y_3|$. The oscillation center becomes a constant for $|y_2 - y_3| \gg 1$. For $t_4 = -0.5, -0.54$, the oscillating part can be attributed to the discreteness barrier of LOR 2.

From Eqs. (31) and (32), one can see that for $|y_2 - y_3| \gg 1$, it should have $\tau_{3,2} \approx 2k^x_{2,3}$. However, the situation is a bit more complicated if the force is studied more carefully. It is found that there is a fine structure for the tension $\tau_{n,n+1}$.

The four cases shown in Figs. 8(a) and 8(c) can be cataloged into two types. The cases $t_4 = -0.3, -0.4$ shown in Fig. 8(a) belong to a type and it has $\rho_2 \ll \tau_{2,3}$. The cases $t_4 = -0.5, -0.54$ shown in Fig. 8(c) belong to another type and it has $\rho_2 \sim \tau_{2,3}$. For $t_4 = -0.3$, the discreteness barrier is $a_2 = 2.39 \times 10^{-7}$ and it generates a force with maximum $\pi a_2 \approx 1.5 \times 10^{-6}$. This can not explain the oscillating amplitude 5.0×10^{-5}. In addition, the discreteness barrier should induce a force proportional to $\pi a_2 \sin(2\pi y_2)$, which can not have the shape of the oscillating part shown in Fig. 8(b). We have tested many cases with very small $\tau_{1,2}, a_2$, we get the similar shapes of oscillating part of generalized force.

We conclude that the oscillating part is a lattice effect. In other words, the tension $\tau_{3,2}$ should be approximately given by

$$\tau_{3,2} \approx 2k^x_{2,3} + b_{2,3}\left[|\cos(\pi y_2)| - \frac{2}{\pi}\right] \tag{38}$$

for y_3 is fixed and $y_2 - y_3 \gg 1$. The above formula satisfies two requirements. First, $\tau_{3,2}$ should be a periodic function with period 1. Second, the averaged $\tau_{3,2}$ should be equal to $2k^x_{2,3}$ [see Eq. (28)], i.e., $\int_{-0.5}^{0.5} \tau_{2,3} dy_2 = 2k^x_{2,3}$.

Figures 8(b) and 8(d) show the agreement of the fine-structure formula (38) with the numerical results. For $t_4 = -0.3$, it has $2k_{2,3} = 6.41 \times 10^{-4}$ and $b_{2,3} = 5.0 \times 10^{-5}$. The scatters are the numerical results and the solid line is drawn according to Eq. (38). For $t_4 = -0.4$ shown in Fig. 8(b), the oscillating part contains the discreteness barrier of LOR 2 and the lattice effect of $\tau_{2,3}$. The solid line is drawn according to Eq. (38) with $2k_{2,3} = 7.22 \times 10^{-4}$, $b_{2,3} = 8.0 \times 10^{-5}$. The numerical result (the scatters) of the transient states agree with Eq. (38) well. It is so for $t_4 = -0.5, 0.54$ shown in Fig. 8(d). The fine-structure coefficient $b_{n,n+1}$ is generally less than 10% of $2k^x_{n,n+1}$. This is tested in a large range of parameters. Therefore, we omit the fine structure in the following discussion.

Now, we summarize the generalized forces as follows. From Eqs. (34) and (35), the discreteness barrier of DW across the LOR n can cause the resistance ρ_n:

$$\rho_n \approx \pi a_n \sin(2\pi y_n). \tag{39}$$

The tensions between the LORs are approximately given by

$$\begin{aligned} &|\tau_{n\pm1,n}| = 2k^x_{n\pm1,n} \quad \text{for } |y_n - y_{n\pm1}| \gg 1, \\ &|\tau_{n\pm1,n}| \to 0 \qquad \text{as } |y_n - y_{n\pm1}| \to 0. \end{aligned} \tag{40}$$

Here, we omit the fine structure due to the lattice effect.

If the DW across LOR 2 is stable, it must be satisfied that $\partial F/\partial y_2 = 0$, i.e., the net force on the DW across LOR 2 is zero. According to Eq. (33), we get

$$\rho_2 + \tau_{12} + \tau_{23} = 0. \tag{41}$$

Specifically, for the big cap case shown in Fig. 7(a), it has $\tau_{1,2},\tau_{3,2} < 0$, $\rho_2 > 0$. Then, we get the balance equation

$$|\rho_2| = |\tau_{12}| + |\tau_{23}|. \tag{42}$$

Because $|\tau_{1,2}| \leqslant 2k^x_{1,2}$, $|\tau_{1,2}| \leqslant 2k^x_{1,2}$, and $\rho_2 \leqslant \pi a_2$, we get that if

$$\pi a_2 > 2k^x_{1,2} + 2k^x_{2,3}, \tag{43}$$

the balance can always be reached in any case. Then, one can find a local minimum of free energy for y_2 in every period of one, as shown in the cases $t_3 = t_5 = 0.1, 0.071$ in Fig. 7(c). Otherwise, one can not find a local minimum as shown in the case $t_3 = t_5 = 0.05$ in Fig. 7(c). One can test it with the parameters given in Table I.

And, for the elbow case shown in Fig. 7(a), it has $\tau_{3,2} > 0$, $\tau_{1,2} < 0$, and $\rho_2 = -(\tau_{1,2} + \tau_{3,2})$:

$$|\rho_2| = ||\tau_{12}| - |\tau_{23}||. \tag{44}$$

Because $|\tau_{1,2}| \leqslant 2k^x_{1,2}$, $|\tau_{1,2}| \leqslant 2k^x_{1,2}$, and $\rho_2 \leqslant \pi a_2$, we get that if

$$\pi a_2 > \left|2k^x_{1,2} - 2k^x_{2,3}\right| \tag{45}$$

the balance can always be reached at a point $j < y_2 < j + 1$ where j is an arbitrary integer. This condition is satisfied for the three cases shown in Fig. 7(d). Then, one can find a local minimum of free energy for y_2 in every period of one, as shown in Fig. 7(d).

To illustrate the generalized forces and the DWs simply, we draw diagrams in Fig. 9. The red lines indicate the DWs. The black dotted lines indicate the borders of LORs. The blue arrows indicate the generalized forces. Figure 9(a) is for the elbow case and 9(b) is for the big cap case. The above relations for the generalized force can be seen simply in the sketches.

These stable conditions (43) and (45) can be extended to any stable DW across a LOR. There is a simple physical explanation for the above equation. The generalized forces from the vertical DWs between LORs tend to shrink the DW. However, the horizontal DWs across the LORs resist the shrinking because of the discreteness barriers. If the barrier is high enough and then the resistance is strong enough, the DW across the LOR can be stable.

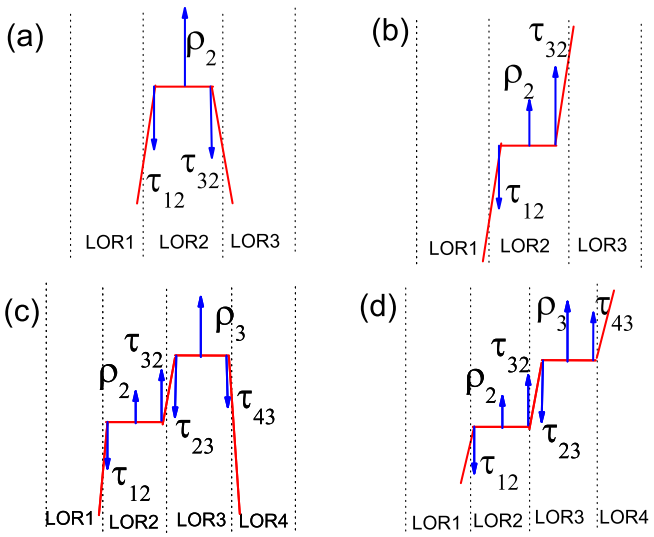

FIG. 9. The sketch of generalized forces. (a) The big cap case. (b) The elbow case. (c) The big cap case with two horizontal DW segments. (d) The elbow case with two horizontal DW segments.

V. THE ELEMENTARY CLUSTER AND ITS CRITERION

A. Elementary cluster and the effective Hamiltonian at the saddle point level

For $\pi a_2 > 2(k^x_{1,2} + k^x_{2,3})$, both the elbow and big cap are stable. The DW segment across the LOR 2 can be stable at the middle between any neighbored rows, i.e., any jth and $(j + 1)$th row. Then, we call LOR 2 an elementary cluster (EC).

To distinguish from the LOR, we denote the quantities of EC with bigger letters. For example, we use $L_N, K^x_{N,N+1}, K^y_N$ to denote the size, the couplings between two neighbored ECs, and the vertical couplings inside an EC. If the condition $\pi a_n > 2(k^x_{n-1,n} + k^x_{k,k+1})$ for all three LORs is satisfied, every LOR is an EC. The couplings between ECs $K^x_{N,N+1}$ and inside ECs K^y_N are just $k^x_{n,n+1}, k^y_n$ because the three LORs are ECs.

The stable DW configurations can be mapped to an Ising model. The three ECs can be regarded as three columns of Ising spins. If the solution has opposite sign in two neighbored LORs, say EC n and $n \pm 1$, there exists a segment of vertical DW of length 1, which causes a free-energy increase $2K^x_{n,n\pm1}$. If the solution changes sign inside an EC, there exists a segment of DW across the EC, which causes a free-energy increase $2K^y_n$. In the horizontal direction, the spatial size of the spin is the size of EC L_n. In the vertical direction, the spatial size of the spin is the original lattice constant. Then, the free-energy increase for a stable excited state solution can be approximately given by

$$H_{\rm sad} = -\sum_{N,j}\left[K^x_{N,N+1}S_{N,j}S_{N+1,j} + K^y_N S_{N,j}S_{N,j+1} - h' M_N S_{N,j}\right], \tag{46}$$

where $S_{N,j} = \pm 1$ is spin of the Nth EC at jth site in the vertical direction, $K^x_{N,N+1}, K^y_N$ are the couplings between ECs. They are just $k^x_{n,n+1}, k^y_n$ because the three LORs are ECs. The magnetic moment of the Nth EC is given by

$$M_N = \sum_{i\in N\text{th EC}} \frac{1}{2}\phi_i. \tag{47}$$

The partition function at the SP level is given by

$$Z = \sum_{\{S_{N,j}\}} e^{-H_{\rm sad}}. \tag{48}$$

In the following, we will show that an EC usually consists of multiple LORs rather than single LOR. In that case, the couplings between ECs $K^x_{N,N+1}$ and inside ECs K^y_N are not $k^x_{n,n+1}, k^y_n$. However, the effective Hamiltonian for the saddle point solution is still given by Eq. (46).

One may note that for a stable excited state solution, two DW segments across the same LOR can not be too close. There should be a minimal distance, just as discussed in Sec. III C. We have studied this distance minimum for some cases. In our concerned situation, the distance minimum can be estimated

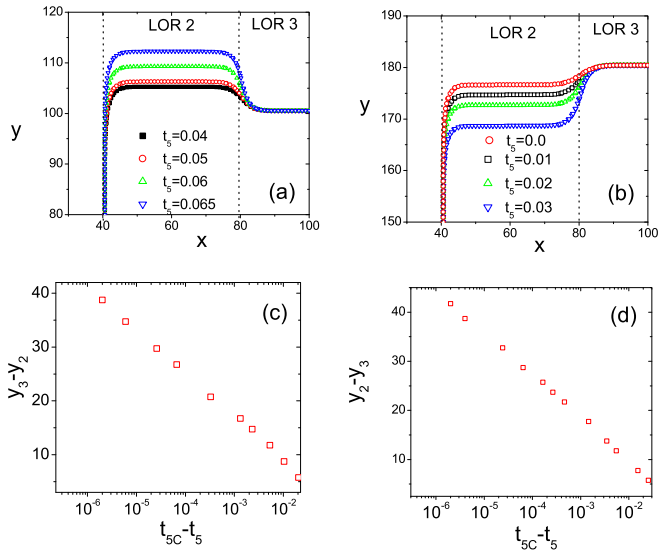

FIG. 10. (a) The stable DW for $2(k^x_{2,3}+k^x_{1,2})>\pi a_2$. (b) The black dotted lines mark the borders of LORs. The stable DW for $2(k^x_{2,3}-k^x_{1,2})>\pi a_2$. (c) The distance between the DW segment across LORs 2 and 3 for case (b) vs t_5 with $t_{5c}=0.070\,326$. (d) The distance between the DW segment across LORs 2 and 3 for case (a) vs t_5 with $t_{5c}=0.035\,464$.

to be $6/|t|$, where t is the reduced temperature at the center of LOR. If K^y_N is much bigger than 1 and the Nth EC is dealt as an isolated Ising chain in vertical direction, the correlation length is given by $e^{2K^y_N}/2$. In other words, the most probable distance between two DW segments across the Nth EC is $e^{2K^y_N}/2$. If this most probable distance is much larger than the minimal distance, this constraint from the minimal distance will not cause much error. This condition is satisfied in the random temperature cases discussed in the following sections.

If $\pi a_2<2(a^x_{2,3}+a^x_{1,2})$ and $\pi a_2>|2(k^x_{2,3}-k^x_{1,2})|$, the DW segment across LOR 2 is not stable in big cap case for $y_2-y_1\gg 1$, $y_2-y_3\gg 1$ but stable in the elbow case. Then, the saddle point solutions can not be described by Eq. (46) any longer. LOR 2 is not an EC. Of course, one adds a constraint to eliminate the DW configuration containing big cap at LOR 2 in Eq. (46).

B. Near the unstable point of EC

For the big cap case as shown in Fig. 10(a), the DW segment across LOR 2 is not stable for $y_2-y_3\gg 1$ any longer if $\pi a_2<2(k^x_{2,3}+k^x_{1,2})$. In this case, the DW segment across LOR 2 will be dragged to the DW segment across LOR 3. However, as the distance y_2-y_3 decreases, it may become stable. Figure 10(a) shows such a situation in four cases with $2(k^x_{2,3}+k^x_{1,2})>\pi a_2$. In these cases, a_2,$k^x_{1,2}$ are fixed and $k^x_{2,3}$ is different since it depends on t_5. The smaller t_5 is, the stronger $k^x_{2,3}$ is. The main part of the DW segment between LORs 2 and 3 is inclined. The tension $\tau_{2,3}$ on this inclined DW is less than $2k^x_{2,3}$, so the balance can be reached as the DW is inclined enough. See the case for $t_5=0.065$ shown in Fig. 10(a), where the DW segment across LOR 3 is stable and its vertical position is given by $y_3\approx 100.5$ for $x=100$. The DW segment across LOR 2 is unstable if we set its initial position $y_2>113$ for $x=60$. The solution will converge to $y_2=112.273$ for $x=60$. $y_2-y_3\approx 11.7$ is the maximal difference between the y coordinates of the DW segments across LORs 2 and 3. Moreover, there are stable solutions for $0<y_2-y_3<11$ since the DW segment between LORs 2 and 3 is more inclined and $\tau_{2,3}$ becomes smaller.

We adjust $k^x_{2,3}$ through tuning t_5. As t_5 approaches the critical value t_{5C}, the maximum stable distance y_2-y_3 increases to infinity logarithmically obeying

$$|y_{03}-y_{02}|_{\max}\sim\log|t_{5C}-t_5|. \tag{49}$$

This logarithmic dependence is shown in Fig. 10(c). This indicates that unless πa_2 is very close to $2(k^x_{2,3}+k^x_{1,2})$, the distance y_2-y_3 is small and in order of 1.

For the elbow case as shown in Fig. 10(b), the DW segment across LOR 2 is not stable if $\pi a_2<2(K^x_{2,3}-K^x_{1,2})$. In this case, the DW segment across LOR 2 will be dragged to the DW segment across LOR 3. Figure 10(b) shows the stable location of the DW segment across LOR 2 in four cases with $\pi a_2<2(k^x_{2,3}-k^x_{1,2})$. In these cases, the main part of the DW segment between LORs 2 and 3 ($70<x<90$) is inclined, rather than vertical. The inclined DW segment between LORs 2 and 3 causes a tension less than $2k^x_{2,3}$, so the balance can be reached. See the case $t_5=0.03$ (the blue triangle scatters), the distance between the DW segments across LORs 2 and 3 is $y_3-y_2=11.758$. If y_2 is set to be $y_3-y_2>12$ initially, the DW segment across LOR 2 is not stable. The solution converges to $y_3-y_2=11.758$. Moreover, there are stable solutions for $0<y_3-y_2<11$ since the DW segment between LORs 2 and 3 is more inclined and $\tau_{2,3}$ is smaller.

If $\pi a_2<2(k^x_{2,3}-k^x_{1,2})$ and πa_2 is very close to $2(k^x_{2,3}-k^x_{1,2})$, the maximum stable distance $|y_3-y_2|$ will become very large. It increases to infinity as t_5 approaches to t_{5C} obeying Eq. (49) as shown in Fig. 10(d). If $2(k^x_{2,3}-k^x_{1,2})\gg\pi a_2$, the y_3-y_2 will be very small and in order of 1.

C. Clustering of two neighbored LORs

As discussed in the above, if $\pi a_2<2k^x_{1,2}+2k^x_{2,3}$, the DW across LOR 2 in the big cap case will be dragged to the DW across LOR 3. Usually, y_2-y_3 is small and in order of 1. If $\pi a_2<2(k^x_{2,3}-k^x_{1,2})$, the DW across LOR 2 in the elbow case will also be dragged to that across 3. y_3-y_2 is small and in order of 1 unless πa_2 is very close to $2(k^x_{2,3}-k^x_{1,2})$. In this case, the DW segments across LORs 2 and 3 can be regarded as being "tied together." The LORs 2 and 3 are united as an EC. To realize such DW configuration, it is required that the superspins $S_{2,j}$ and $S_{3,j}$ flip coherently, where j is row's label. Then, we only have two ECs: the EC of LOR 1 and the EC of LORs 2 and 3. Obviously, the size of this EC is the sum of the sizes of LORs 2 and 3, i.e., $L_2=l_2+l_3$.

If $\pi a_2<2k^x_{1,2}+2k^x_{2,3}$ but $\pi a_2>2(k^x_{2,3}-k^x_{1,2})$, the DW across LOR 2 in the big cap case will be dragged to the DW across LOR 3, but the DW across LOR 2 in the elbow can be stable for $y_3-y_2>0$. In this case, the DWs across LORs 2 and 3 can be regarded to be tied up only in the big cap case rather than in the elbow case. We have two options to deal this situation. One option is to add constraint to eliminate the big cap configuration in the summation of partition function. Another option is to ignore it if the probability of this situation is very small. In the random temperature case, we argue that

the probability of this case is small and plays a less important role. We ignore it in the random temperature cases.

As LORs 2 and 3 form an EC, which is denoted by EC 2, the free-energy increase caused by the DW across it is the effective coupling of the EC in the y direction. It is simply given by

$$K_2^y = k_2^y + k_3^y \tag{50}$$

and its size is given by

$$L_2 = l_2 + l_3. \tag{51}$$

What about the discreteness of the EC of LORs 2 and 3? See the big cap case for the EC of LORs 2 and 3 in Fig. 9(c), if DW segments across LORs 2 and 3, it must have $|\tau_{1,2}| = |\rho_2| + |\tau_{3,2}|$ and $|\tau_{2,3}| + |\tau_{4,3}| = |\rho_3|$. Considering $\tau_{3,2} = -\tau_{2,3}$, we get $|\tau_{1,2}| + |\tau_{4,3}| = |\rho_2| + |\rho_3|$. The stable condition for the DW across this EC should be $\pi(a_2 + a_3) > 2(k_{1,2}^x + k_{3,4}^x)$, so the effective discreteness barrier is given by

$$A_2 = a_2 + a_3. \tag{52}$$

This argument can be applied to the elbow case for the EC of LORs 2 and 3 shown Fig. 9(d). One gets the above equation again. Then, it must be satisfied that

$$\pi A_2 = \pi(a_2 + a_3) > 2K_{1,2}^x + 2K_{2,3}^x, \tag{53}$$

where $K_{1,2}^x = k_{1,2}^x$, $K_{2,3}^x = k_{3,4}^x$ because EC 2 contains LORs 2 and 3 and EC 3 is the previous EC 4. The coupling between ECs 1 and 2 is $k_{1,2}^x$ and that between ECs 2 and 3 is $k_{3,4}^x$.

In the cases shown in Fig. 10(b), the LOR 2 can not be an EC but LOR 3 can be an EC. They are united as a new EC. The DW across LOR 2 is dragged to that across LOR 3. Here, the necessary condition to is $2k_{2,3}^x > 2k_{1,2}^x + \pi a_2$. Of course, if the LOR 3 can not be an EC but LOR 2 can be an EC and $2k_{2,3}^x > 2k_{3,4}^x + \pi a_3$, LORs 2 and 3 are also united as a new EC. The DW across LOR 3 will be dragged to that across LOR 2. There is another possibility. If both LORs 2 and 3 can not be ECs, but $\pi(a_2 + a_3) > 2k_{1,2}^x + 2k_{3,4}^x$, they may be united as an EC. The coupling between LORs 2 and 3 is strong enough to drag the DWs across LORs 2 and 3 together.

Therefore, aside from the stability condition (53), there is another sufficient condition, that is, $k_{2,3}^x > k_{1,2}^x$ or $k_{2,3}^x > k_{3,4}^x$. So, the tension from the DW between LORs 2 and 3 can drag the DW across LORs 2 and 3 together. In other words, the coupling between LORs inside an EC should be larger than the couplings between this EC and its neighbors, which are the coupling between the LOR at the its left border and the LOR in the left neighbored EC, and that between the LOR at its right border and the LOR in the right neighbored EC.

Generalizing the above discussion, one can get the following rules.

(1) The y-direction coupling for this EC is given by

$$K_N^y = \sum_i k_n^y, \ n \in \text{the } N\text{th EC}. \tag{54}$$

(2) Its size is given by

$$L_N = \sum_n l_n, \ n \in \text{the } N\text{th EC}. \tag{55}$$

(3) Its magnetic moment is given by

$$\tilde{m}_N = \sum_n \varphi_n, \ n \in \text{the } N\text{th EC}. \tag{56}$$

(4) For this EC, the effective discreteness barrier is given by

$$A_N = \sum_n a_n, \ n \in \text{the } N\text{th EC}. \tag{57}$$

(5) The couplings with its neighbored ECs are given by

$$K_{N-1,N}^x = k_{NL}^x; \quad K_{N,N+1}^x = k_{NR}^x, \tag{58}$$

where k_{NR}^x, k_{NL}^x are the couplings between the leftmost and the rightmost LOR of the Nth EC with their neighbored LORs in other ECs.

(6) The criterion of the stability for this EC is that the effective resistance must be larger than the sum of the tensions of the leftmost and the rightmost boundaries:

$$\pi A_N > 2\left(K_{N-1,N}^x + K_{N,N+1}^x\right). \tag{59}$$

Moreover, in this EC there should not be a subgroup of adjoined LORs satisfying the above equation. Otherwise, the cluster is not elementary.

(7) Aside from this necessary stability condition, there is another necessary condition. To drag the DWs across LORs in the EC, the couplings between LORs inside an EC should be larger than one of the couplings $K_{N-1,N}^x + K_{N,N+1}^x$, between this EC and its neighbors.

VI. SADDLE POINT SOLUTION WITH RANDOM TEMPERATURE

Now, we report the result of the saddle point (5) with random temperatures with the following form:

$$t_i = t_0 + \delta t_i, \tag{60}$$

where $\tilde{t}_i$ obeys a uniform distribution

$$p(\delta t_i) = \frac{1}{w}, \quad -\frac{w}{2} \leqslant \tilde{t}_i \leqslant \frac{w}{2}. \tag{61}$$

See the transformation (3); the random temperature in Eq. (5) is a transformed one. Its width is $z = 4$ times the original one. We consider three cases with original widths 0.5,0.4,0.3, which are narrow, so the widths of the transformed random temperature in Eq. (5) are set to be $w = 2.0, 1.6, 1.2$.

To explain our algorithm, we show a typical ground state solution (the solid green line) in Fig. 11(a). After getting the ground state solution, we divide the system into LORs. The algorithm to determine the boundary of LOR is as follows. From the right boundary of the last LOR, we search the local maximum of the next $l_s = 20$ sites. Then, from the maximum, we search the local minimum of the next $l_s = 20$ sites. The position of this minimum is the right boundary of this LOR. Reiterating the process to scan over the whole system, we get all the LORs. The boundaries of LOR are shown with blue drop lines in Fig. 11(b). Then, we calculate the couplings $2k_{n,n+1}^x$ between two neighbored LORs according to Eq. (28) and the coupling inside a LOR $2k_n^y$ and the discreteness barrier a_n of each LOR according to Eqs. (29) and (30). In these calculations, the vertical size in solving a_n, k_n^y is set to be 300.

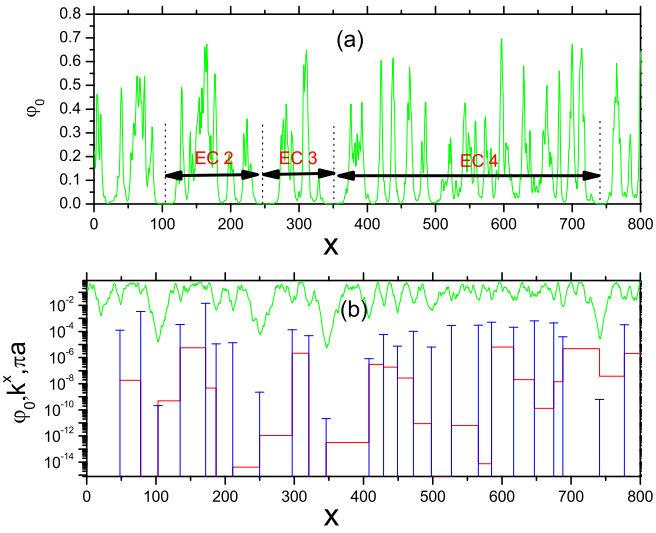

FIG. 11. (a) The solid green curve is the ground state solution. The ranges of three ECs are indicated by the black dotted lines. (b) The blue drop lines are the boundaries of LORs and the tops are the x-direction couplings between two adjoined LORs $2k^x_{n,n+1}$. The red horizontal segments are the discreteness barriers of the LORs πa_n. These results are obtained with $w = 2.0$, $t_0 = 0.2$ of the transformed random temperature.

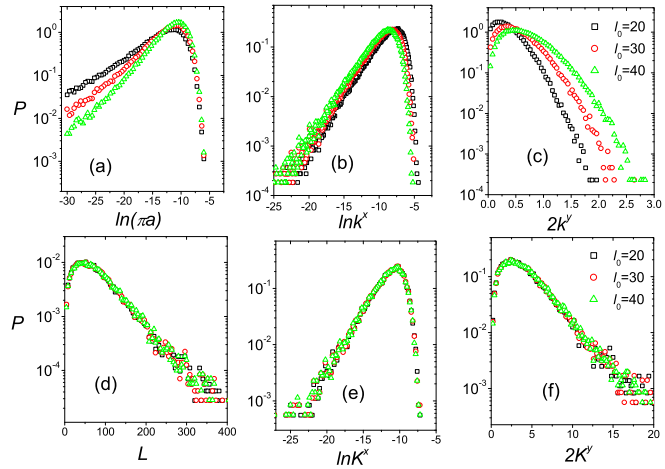

FIG. 12. The distributions of LOR sizes l_n, the couplings $k^x_{n,n+1}$,k^y_n. The distributions of cluster sizes L_N, the couplings $K^x_{N,N+1}$,K^y_N. These results are obtained with $w = 2.0$, $t_0 = 0.0$ of the transformed random temperature.

At last, we determine the ECs according to Eq. (59). In the lower panel, we show the couplings $k^x_{n,n+1}$ between LORs by the blue drop lines and the discreteness barriers πa_n by red steplike lines. As one can see, most of $k_{n,n+1}$ are much larger than πa_n. Usually, a single LOR can not form an EC, and an EC usually has many LORs. At about $x = 100,250,350,740$, where the ground state solution is almost zero, the couplings $k^x_{n,n+1}$ are small enough to satisfy Eq. (59) to form ECs. Therefore, for the ECs 2,3,4, the boundaries are at about $x = 100,250,350,740$ as shown in the upper panel.

We search the maximum and minimum in the next $l_s = 20$ sites. The parameter l_s for finding the LOR has some arbitrariness. We will show that the distributions for ECs do not depend on this parameter. In Fig. 11, the LORs are found with $l_s = 20$. In fact, one can set other l_s, for example, $l_s = 30,40$. Obviously, with different l_0, one will get different LORs. However, we find that the distributions for the ECs are almost the same. This is shown in Fig. 12. In the upper panels, the distributions of discreteness barrier a_n, the couplings $k^x_{n,n+1}$,k^y_n for LORs are shown. Obviously, they are different for different l_s. However, the distributions of size, the couplings $K^x_{N,N+1}$,K^y_N for ECs collapse for $l_s = 20,30,40$, are shown in the lower panels. In other words, the distributions for EC do not depend on the parameter l_s. To get the distribution of the ECs, 300 samples are made. Each sample is a lattice with 50 000 sites, on which we solve the ground state solution of Eq. (27).

A remarkable result is that near $t_0 = 0$ the couplings K^y_N inside ECs are very strong and the couplings $K^x_{N,N+1}$ between ECs are very weak. Moreover, the size of ECs is usually much larger than that of LORs. There is a simple reason for this situation. As shown in Figs. 12(a) and 12(b), the discreteness barriers for most LORs are very small and smaller than most couplings between LORs, and only a small part of LORs have discreteness barriers larger than a small part of couplings between LORs. Therefore, usually multiple LORs can form an EC. The average size of LORs is less than $2l_s = 40,60,80$. As shown in Fig. 12, the average size of EC is 278, much larger than that of LORs and the size distribution of ECs has an exponential tail for large size. In addition, the size distributions of ECs collapsed for different l_s.

As shown in Figs. 12(b) and 12(e), the average of k^x is much larger than K^x. This can guarantee the necessary condition 7 after Eq. (59) that the couplings between LORs inside an EC should be larger than one of the couplings $K^x_{N-1,N} + K^x_{N,N+1}$, between this EC and its neighbors.

In this case, the effective Hamiltonian for the EC is an extremely anisotropic two-dimensional Ising model with extremely strong vertical bonds and extremely weak horizontal bonds. It can be mapped to a one-dimensional transverse-field Ising model (TFIM) [27,28]

$$H_{\mathrm{TFIM}} = -\sum_N \left(J_{N,N+1}\sigma^z_I\sigma^z_{N+1} + \gamma_N\sigma^x_N\right), \tag{62}$$

where

$$J_{N,N+1} = K^x_{N,N+1}, \quad \gamma_N = e^{-2K^y_N}. \tag{63}$$

According to the result of TFIM, the critical point is given by $\overline{\ln J} = \overline{\ln \gamma}$ [8]. Therefore, the critical point for the effective Hamiltonian for the EC is given by

$$-\overline{\ln K^x} = 2\overline{K^y}. \tag{64}$$

We can determine the critical point of the effective Hamiltonian at the saddle point level according to the above equation. For $w = 2.0$, we get $t_C = -0.1565$, at which it has $-\overline{\ln K^x} = 2\overline{K^y} = 8.613$ and $\overline{L} = 288$. For $w = 1.6$, we get $t_C = -0.077\,44$, at which it has $-\overline{\ln K^x} = 2\overline{K^y} = 10.97$ and $\overline{L} = 700$. For $w = 1.2$, we get $t_C = -0.0241$, at which it has $-\overline{\ln K^x} = 2\overline{K^y} = 14.73$ and $\overline{L} = 2100$.

A qualitative trend is that as the width w decreases, the average $-\overline{\ln K^x} = 2\overline{K^y}$ and the average size of EC increases. Moreover, the average $2\overline{K^y}$ is much larger than 1, so the

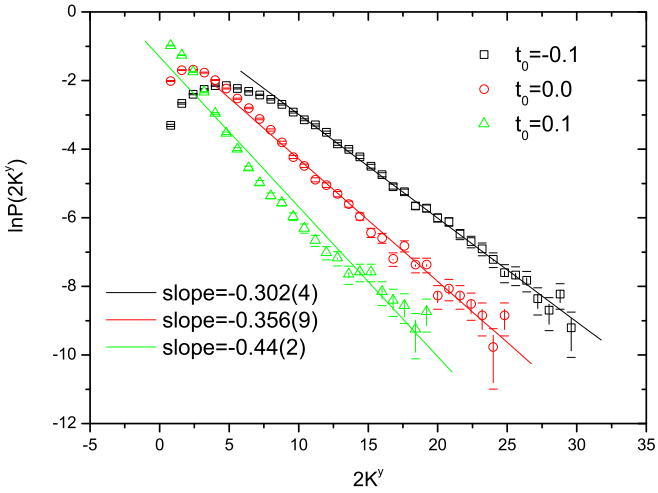

FIG. 13. The distributions of vertical bond $2K^y$. These results are obtained with $w = 2.0$ of the transformed random temperature.

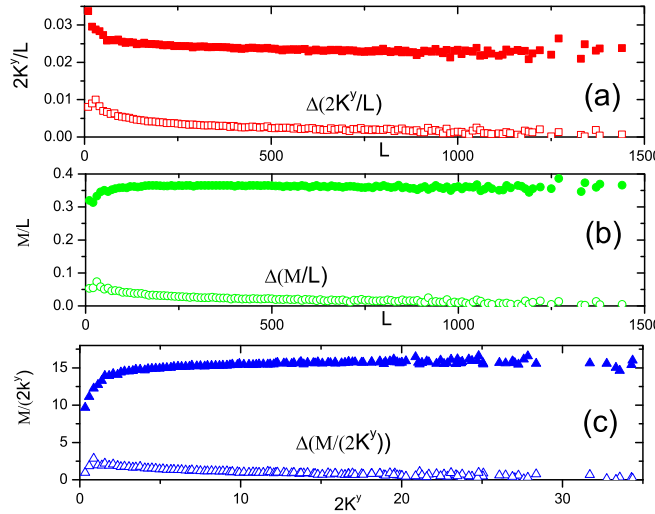

FIG. 14. The relation between $2K^y$ and the size of EC and magnetic moment of EC. The solid scatters are the average of $2K_N^y/L_N, M_N/L_N, M/(2K_N^y)$ and empty scatters are the deviations (the distribution width) of the corresponding quantities. These results are obtained with $w = 2.0$, $t_0 = -0.1$ of the transformed random temperature.

most probable distance between two horizontal DWs, which is approximately given by e^{2K^y}, is much bigger than 1.

We have also carried out the numerical calculation for the binary distribution of random temperature. The properties are the qualitatively the same as those for the uniform distribution. We do not present the results here.

Griffiths-McCoy singularity

The Griffiths-McCoy singularity is found in the McCoy-Wu model [4], at both sides of the critical point, where the susceptibility is divergent in a whole region.

As shown above, the horizontal bonds are very weak and the vertical bonds are very strong. If the horizontal bonds are ignored, the system can approximately be dealt as isolated chains in vertical direction. Taking a very small field into account, the Ising chain is given by

$$H_{\text{Ising chain}} = \sum_j \left(- K_N^y S_j S_{j+1} - h' M_N S_j \right). \tag{65}$$

For this Ising chain, the magnetization is given by

$$\overline{S_N} = \frac{M_N \sinh(h' M_N)}{L_N \sqrt{e^{-4K^y} + \sinh^2(h' M_N)}}. \tag{66}$$

As shown in Fig. 13, the distribution of K_N^y is exponential in a range of t_0. For large K^y, the distribution can be approximately given by

$$P(K^y) \approx P_0 e^{-2\Gamma K^y}. \tag{67}$$

In Fig. 13, for $t_0 = -0.1, 0.0, 0.1$, the indices Γ are 0.302(4), 0.356(9), 0.44(2), respectively. To get these distributions of the ECs, 300 samples are made. Each sample is a lattice with 50 000 sites, on which we solve the ground state solution of Eq. (27).

The relation between K_N^y and M_N is shown in Fig. 14. The size distribution of EC is exponential too. The coupling K^y is approximately proportional to the size of EC as shown in Fig. 14(a). On the other hand, the magnetic moment is also approximately proportional to the size as shown in Fig. 14(b). Therefore, the magnetic moment is proportional to K^y approximately as shown in Fig. 14(c). Then, we can take the approximation

$$M_N \approx 2c_1 K_N^y \approx c_2 L. \tag{68}$$

Combining the distribution of K^y, we get the average magnetization over the whole system as given by

$$\overline{S} = \int \frac{c_2 P_0 e^{-2\Gamma K^y} \sinh(2c_1 h' K^y) dK^y}{\sqrt{e^{-4K^y} + \sinh^2(2c_1 h' K^y)}} \propto h^{\Gamma}. \tag{69}$$

Hence, we get the susceptibility

$$\chi = \frac{\partial \overline{S}}{\partial h} \propto h^{\Gamma - 1}. \tag{70}$$

As shown in Fig. 2, the exponent Γ is less than 1 in a range of temperature. In this regime, the susceptibility is divergent. Obviously, the divergence comes from the ECs with extremely large vertical bond. These ECs have extremely large sizes and exponentially small probability. They are the so-called rare regions.

This approach is similar to the droplet theory for the quantum Ising spin glass proposed by Thill and Huse [6], in which the divergence is attributed to the rare regions. Concerning the role of rare regions in the quantum phase transition in disordered systems, please see the review by Vojta [1]. Our result agrees with these previous theories.

Here, we ignore the horizontal bonds, so we give the lower bounds for the susceptibility divergence since the correlation between superspins will be enhanced if the horizontal bonds are taken into account. In fact, only if the horizontal bonds are taken into account, the long-range order can be realized.

VII. SUMMARY

We have solved the saddle point equation of Landau-Ginzburg-Wilson Hamiltonian for the McCoy-Wu random Ising model. In the saddle point solutions, the LORs self-organize into ECs with a broad size and bond distribution. This leads to the Griffiths-McCoy singularity directly. Our work agrees with the exact solution [4] and the strong-disorder renormalization group theory [7,8]. This result is surprising since it is believed implicitly for 50 years that the saddle point solution can not deal the McCoy-Wu model.

This work indicates that solving the saddle point solution is an efficient approach to understand the phase transition in this kind of disordered system. Its success implies that the saddle point solution may be also an efficient way to study the other disordered systems. It is well known that the saddle point equation is the starting point for the theoretical study on many disordered quantum systems [22]. Understanding the saddle point solution thoroughly in those systems should be interesting.

For the pure system, the saddle point solution is of mean field and the excited state saddle point solutions can be ignored. For the McCoy-Wu model, the saddle point solution is not of the usual mean field and the excited state solutions can not be neglected. Moreover, we show that the discreteness is important for this kind of disordered system and we can not deal the saddle point solution in the continuum limit simply.

The approach in this work can be extended to three-dimensional Ising model with disorder strongly correlated in one dimension, which corresponds to the two-dimensional transverse-field Ising model.

APPENDIX: LGW HAMILTONIAN FOR RANDOM BOND ISING MODEL

We consider the two-dimensional nearest-neighbored Ising model with random bond

$$H = -\frac{1}{2}\sum_{\mathbf{r},\eta} J_{\mathbf{r},\mathbf{r}+\eta} S_{\mathbf{r}} S_{\mathbf{r}+\eta} - h\sum_{\mathbf{r}} S_{\mathbf{r}}, \tag{A1}$$

where $\mathbf{r}$ labels the lattice sites and $\eta = (\pm 1,0),(0,\pm 1)$. Using Stratonovich-Hubbard transformation, we get the effective action

$$S[\phi] = \frac{\beta}{2}\sum_{\mathbf{r},\eta} J_{\mathbf{r},\mathbf{r}+\eta}\phi_{\mathbf{r}}\phi_{\mathbf{r}+\eta} - \sum_{\mathbf{r}} \ln\left[2\cosh\left(\beta h + \beta\sum_{\eta} J_{\mathbf{r},\mathbf{r}+\eta}\phi_{\mathbf{r}+\eta}\right)\right]. \tag{A2}$$

Truncating the expansion of the second term at fourth order, we obtain

$$S[\phi] = \frac{\beta}{2}\sum_{\mathbf{r},\eta} J_{\mathbf{r},\mathbf{r}+\eta}\phi_{\mathbf{r}}\phi_{\mathbf{r}+\eta} - \frac{\beta^2}{2}\sum_{\mathbf{r}}\left[\sum_{\eta} J_{\mathbf{r},\mathbf{r}+\eta}\phi_{\mathbf{r}+\eta} + h\right]^2 + \frac{\beta^4}{12}\sum_{\mathbf{r}}\left[\sum_{\eta} J_{\mathbf{r},\mathbf{r}+\eta}\phi_{\mathbf{r}+\eta} + h\right]^4. \tag{A3}$$

We write $J_{\mathbf{r},\mathbf{r}+\eta} = J + \tilde{J}_{\mathbf{r},\mathbf{r}+\eta}$, where J is the average and $\tilde{J}_{\mathbf{r},\mathbf{r}+\eta}$ is the fluctuating part. Then, the first term becomes

$$\begin{aligned} J_{\mathbf{r},\mathbf{r}+\eta}\phi_{\mathbf{r}}\phi_{\mathbf{r}+\eta} &= -\frac{1}{2}(J + \tilde{J}_{\mathbf{r},\mathbf{r}+\eta})\left[(\phi_{\mathbf{r}} - \phi_{\mathbf{r}+\eta})^2 - \phi_{\mathbf{r}}^2 - \phi_{\mathbf{r}+\eta}^2\right] \\ &\approx \frac{1}{2}(J + \tilde{J}_{\mathbf{r},\mathbf{r}+\eta})\left(\phi_{\mathbf{r}}^2 + \phi_{\mathbf{r}+\eta}^2\right) + \frac{J}{2}(\phi_{\mathbf{r}} - \phi_{\mathbf{r}+\eta})^2, \end{aligned} \tag{A4}$$

where we omit the term $\tilde{J}_{\mathbf{r},\mathbf{r}+\eta}(\phi_{\mathbf{r}} - \phi_{\mathbf{r}+\eta})^2$ since it is of higher order. Similarly, we adopt the approximation for the second term

$$\begin{aligned} \sum_{\eta} J_{\mathbf{r},\mathbf{r}+\eta}\phi_{\mathbf{r}+\eta} &= \sum_{\eta}(J + \tilde{J}_{\mathbf{r},\mathbf{r}+\eta})[\phi_{\mathbf{r}} + (\phi_{\mathbf{r}+\eta} - \phi_{\mathbf{r}})] \\ &\approx \left(zJ + \sum_{\eta}\tilde{J}_{\mathbf{r},\mathbf{r}+\eta}\right)\phi_{\mathbf{r}} + J\sum_{\eta}(\phi_{\mathbf{r}+\eta} - \phi_{\mathbf{r}}), \end{aligned} \tag{A5}$$

where $z = 4$ is the coordination number. Then, we have

$$\left(\sum_{\eta} J_{\mathbf{r},\mathbf{r}+\eta}\phi_{\mathbf{r}+\eta}\right)^2 = \left(z^2J^2 + 2zJ\sum_{\eta}\tilde{J}_{\mathbf{r},\mathbf{r}+\eta}\right)\phi_{\mathbf{r}}^2 + 2zJ^2\sum_{\eta}(\phi_{\mathbf{r}+\eta} - \phi_{\mathbf{r}})\phi_{\mathbf{r}}. \tag{A6}$$

Substituting Eqs. (A4) and (A6) into (A3), we obtain

$$S[\phi] = \sum_{\mathbf{r}}\left[\frac{1}{2z}\sum_{\eta}\frac{(\phi_{\mathbf{r}+\eta} - \phi_{\mathbf{r}})^2}{2} + \frac{t_0 + \delta t_{\mathbf{r}}}{2}\phi_{\mathbf{r}}^2 + u\phi_{\mathbf{r}}^4 - \beta h\phi_{\mathbf{r}}\right], \tag{A7}$$

where $u = \frac{1}{12}$ and

$$\beta_C zJ = 1, \quad t_0 = \frac{T - T_C}{T}, \quad \delta t_{\mathbf{r}} = -\frac{1}{z}\sum_{\eta}\frac{\tilde{J}_{\mathbf{r},\ \mathbf{r}+\eta}}{J}. \tag{A8}$$

[1] T. Vojta, J. Phys. A: Math. Gen. **39**, R143 (2006).
[2] B. M. McCoy and T. T. Wu, Phys. Rev. Lett. **21**, 549 (1968).
[3] B. M. McCoy and T. T. Wu, Phys. Rev. **176**, 631 (1968).
[4] B. M. McCoy, Phys. Rev. Lett. **23**, 383 (1969).
[5] R. Shankar and G. Murthy, Phys. Rev. B **36**, 536 (1987).
[6] M. J. Thill and D. A. Huse, Phys. A (Amsterdam) **214**, 321 (1995).
[7] D. S. Fisher, Phys. Rev. Lett. **69**, 534 (1992).
[8] D. S. Fisher, Phys. Rev. B **51**, 6411 (1995).
[9] A. P. Young and H. Rieger, Phys. Rev. B **53**, 8486 (1996).
[10] C. Pich, A. P. Young, H. Rieger, and N. Kawashima, Phys. Rev. Lett. **81**, 5916 (1998).
[11] O. Motrunich, S. C. Mau, D. A. Huse, and D. S. Fisher, Phys. Rev. B **61**, 1160 (2000).
[12] R. Juhasz and F. Igloi, Phys. Rev. E **66**, 056113 (2002).
[13] J. Hooyberghs, F. Igloi, and C. Vanderzande, Phys. Rev. Lett. **90**, 100601 (2003).
[14] J. Hooyberghs, F. Igloi, and C. Vanderzande, Phys. Rev. E **69**, 066140 (2004).
[15] T. Vojta and M. Dickison, Phys. Rev. E **72**, 036126 (2005).
[16] T. C. Lubensky, Phys. Rev. B **11**, 3573 (1975).
[17] J. Rudnick, Phys. Rev. B **18**, 1406 (1978).
[18] D. Andelman and A. Aharony, Phys. Rev. B **31**, 4305 (1985).
[19] S. M. Dorogovtsev, Sov. Phys.–Solid State **22**, 188 (1980) [Fiz. Tverd. Tela (Leningrad) **22**, 321 (1980)].
[20] D. Boyanovsky and J. L. Cardy, Phys. Rev. B **26**, 154 (1982).
[21] L. D. Cesare, Phys. Rev. B **49**, 11742 (1994).
[22] D. Belitz and T. R. Kirkpatrick, Rev. Mod. Phys. **66**, 261 (1994).
[23] V. Dotsenko, A. B. Harries, D. Sherrington, and R. B. Stincombe, J. Phys. A: Math. Gen. **28**, 3093 (1995).
[24] X. T. Wu, Phys. Rev. B **79**, 184208 (2009).
[25] X. T. Wu, Phys. A (Amsterdam) **495**, 94 (2018).
[26] H. Schmidt and F. Schwabl, Z. Phys. B **30**, 197 (1978).
[27] V. Gurarie, Advanced-statistical-mechanics, https://www.colorado.edu/physics/phys7240/phys7240_sp04/Week3.pdf.
[28] M. Suzuki, Prog. Theor. Phys. **56**, 1454 (1976).